scientific reports

Check for updates

OPEN

Coastal wetland deposition of cathode metals from the world's largest lithium-ion battery fire

Ivano W. Aiello[1]✉, Charlie Endris[1], Steven Cunningham[1], Monique Fountain[2], Maxime M. Grand[1], Wesley Heim[1], Amanda S. Kahn[1] & Kerstin Wasson[2]

Fires at lithium-ion battery storage facilities pose emerging environmental risks that remain largely undocumented under real-world conditions. Following a major fire at the world's largest Battery Energy Storage System (BESS) in Moss Landing, California, we conducted rapid, high-resolution soil surveys to quantify metal fallout in adjacent estuarine wetlands. Field-portable X-ray fluorescence (FpXRF), validated by SEM/EDS, laboratory XRF, and ICP-MS, revealed a significant but transient surface enrichment of nickel (Ni), manganese (Mn), and cobalt (Co). This enrichment had Ni: Co mass ratios near 2:1 serving as a geochemical fingerprint of NMC-type cathode materials. The metals were confined to a shallow surface layer (< 5 mm). Surface concentrations declined rapidly following precipitation and tidal inundation. The fallout's thin, transient and patchy distribution would have eluded standard coring methods but was detected through spatially intensive FpXRF sampling, highlighting the importance of rapid detection and the mobilization of metals into wetland ecosystems. These findings underscore the need for adaptive environmental monitoring following battery fires and raise critical considerations for ecosystem protection and infrastructure as energy storage systems expand.

Rapid growth of distributed energy storage systems in recent years reflects the global need to store power from renewable energy sources and to regulate electrical systems[1–3]. Lithium-ion batteries (LIBs) are the most widely used type of electrochemical energy storage, as they offer high energy and power density compared to other battery technologies[4]. However, electrochemical energy storage and the use and disposal of LIBs involves inherent risks, such as thermal runaway[5] which can lead to the release of potentially toxic compounds from battery materials[6], and localized deposition of battery-associated metals in adjacent ecosystems[7], with, potentially, long-term implications for terrestrial, aquatic, and human health.

Establishing robust environmental baselines in areas surrounding energy storage systems and achieving adequate spatial and temporal coverage to identify contamination after emergency release are both logistically difficult and often cost-prohibitive. In this context, portable and cost-effective technology such as X-ray fluorescence (FpXRF) offers a means of collecting high-density data, serving as a valuable complement to traditional laboratory-based analytical methods.

On 16 January 2025, a large fire engulfed the largest lithium-ion battery (LIB) Battery Energy Storage System (BESS) in the world, burning actively for at least 2 days. This was followed by a smaller reignition on 18 February 2025. Owned by Vistra Corporation, the BESS is in Moss Landing, California, immediately adjacent to Elkhorn Slough, a Ramsar site recognized as a wetland of international importance[8]. The fire affected the core of the facility (Phase 1) which had a capacity of 300 MW/1200 megawatt-hours (MWh) and was equipped with LG Energy Solution's TR1300 battery rack systems[9]. The fire destroyed approximately 75% of the facility[10] and produced a smoke plume visible from tens of kilometers away, depositing ash and soot across the surrounding area (Fig. 1a). Due to potential toxicity, including possible exposure to hydrogen fluoride, evacuation orders and road closures were issued. Residents were permitted to return 2 days after the fire began[11].

Controlled experiments show Li-ion battery fires emit metal-bearing aerosols (notably Ni–Co–Mn) and other toxicants, which can deposit downwind[6]. Three days after the fire, we rapidly mobilized to assess whether surface soils at Hester Marsh, a wetland restoration area within the Elkhorn Slough National Estuarine Research Reserve (ESNERR), only a few km from the Moss Landing facility had been affected by the fallout material from the smoke plume. Coincidentally, we had collected baseline surface soil elemental data in the same area for other research purposes with an FpXRF in 2023 (Fig. 2).

[1]Moss Landing Marine Laboratories, San Jose State University, 8272 Moss Landing Rd., Moss Landing, CA 95039, USA. [2]Elkhorn Slough National Estuarine Research Reserve, 1700 Elkhorn Road, 95076 Royal Oaks, CA, USA. ✉email: ivano.aiello@sjsu.edu

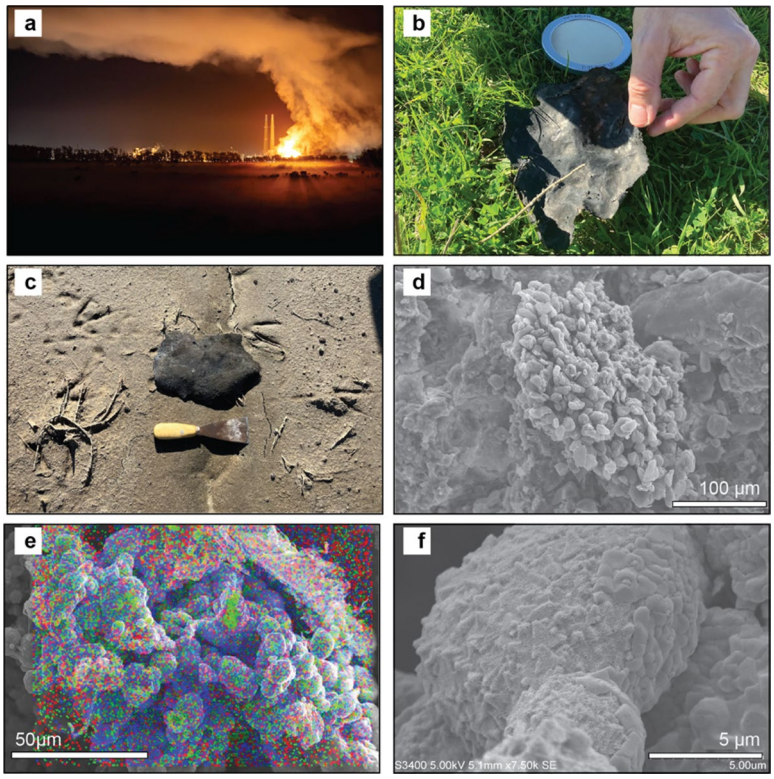

Fig. 1. (**a**) Photo of the battery fire and the smoke plume on January 16th, 2025. The picture is looking south towards the smokestacks of the old Moss Landing power plant and shows the smoke plume hovering Elkhorn Slough and Hester marsh to the east (Photo credit: Mike Takaki). (**b**–**c**) Field photographs showing burned battery fragments from the Vistra battery facility fire collected near transect T12 (B) and transect T8 (C). (**d**) Scanning electron microscope (SEM) images of cathode material aggregate composed of multiple Nickel Manganese Cobalt (NMC) microparticles; (**e**) Energy-dispersive X-ray spectroscopy (EDS) elemental map highlighting the spatial distribution of nickel (Ni, red), manganese (Mn, blue), and cobalt (Co, green). (**f**) A SEM close-up of a single NMC particle.

The Moss Landing battery facility is located within a complex and vulnerable landscape. It sits adjacent to Elkhorn Slough, one of California's largest estuaries, near the town of Moss Landing, and is surrounded by intensively farmed agricultural land. The fallout from the fire's smoke plume raises serious concerns about contamination of soils, water, and vegetation in this region.

Here, we report on the extent and dynamics of cathode metal contamination in estuarine soils immediately following the world's largest lithium-ion battery fire. By combining rapid, high-resolution field surveys with laboratory validation, we tracked the deposition and short-term fate of battery-derived metals in a sensitive wetland ecosystem. Our findings provide rare real-world evidence of the environmental footprint of large-scale battery fires, underscore the value of having a baseline near industrial sites that pose contamination risks, and demonstrate the utility of FpXRF as a practical tool for rapid and spatially intensive environmental monitoring.

Specifically, we test whether the Moss Landing fire deposited a thin surface veneer of battery-associated metals in adjacent wetlands that differ relative to 2023 baseline conditions and whether composition is consistent with NMC cathode material, using a high-density FpXRF survey validated with SEM/EDS, LpXRF, and ICP-MS.

Study area and methodology

Elkhorn Slough is a tide-dominated estuary that in the past 150 years has lost significant vegetated marsh area[12]. At Hester Marsh, extensive diking and draining caused the area to subside and degrade to unvegetated mudflat. In 2018, ESNERR initiated a restoration project to reestablish healthy marsh ecosystems through soil addition, creating a high elevation marsh plain that is only inundated by the highest tides.

To assess relationships between marsh plant health and soil composition, soil property analyses including elemental analysis with a portable Hitachi XMET 8000 XRF (pXRF), were conducted in 2023 along ten permanent transects also monitored for vegetation. These compositional data serve as a baseline for elemental concentrations in soils prior to the 2025 battery fire (Table 1). Following the 16 January 2025 fire at the Moss Landing battery storage facility, three of the original transects were resampled at high spatial and temporal resolution between 21 January and 23 February 2025 (Tables S1 and S2).

During the 2023 survey, surface and subsurface (~5–10 mm depth) samples were collected to compare elemental concentrations above and below the shallow redox boundary characteristic of these tidal marsh soils.

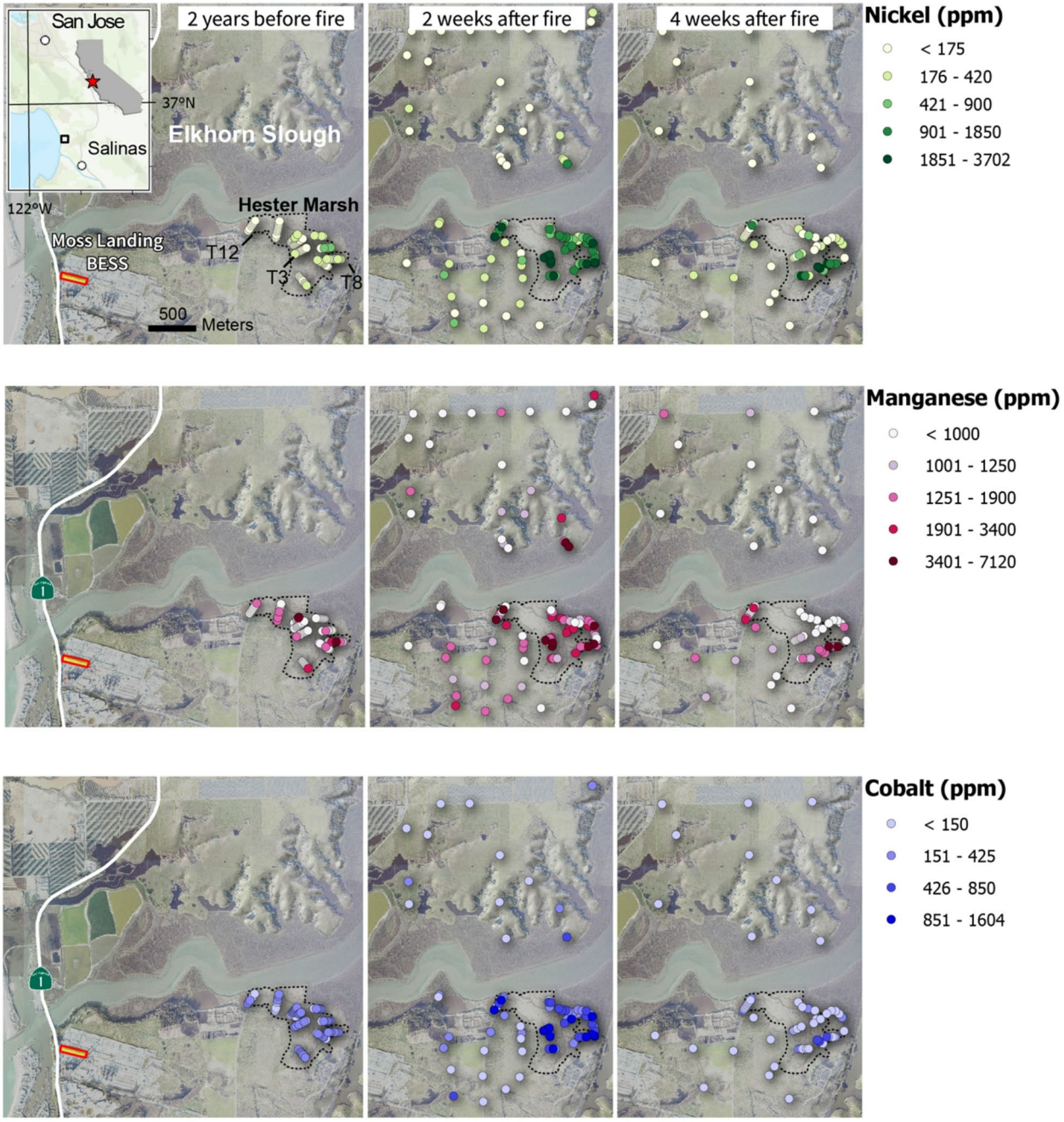

Fig. 2. Spatial distribution of nickel (Ni), cobalt (Co), and manganese (Mn) concentrations (ppm) in soils across three survey periods. The Hester Marsh restoration area is outlined with a dashed line and includes the locations of transects T12, T3, and T8. Peak concentrations were detected within this zone, approximately 1–3 km downwind of the Moss Landing battery facility. Color scales are consistent across all time points for each element to allow temporal comparison. Point classification for each element was done using the "Natural Breaks" (Jenks) method. The map was generated using ArcGIS Pro v3.4.2 (https://pro.arcgis.com/en/pro-app/latest/get-started/download-arcgis-pro.htm).

Additional measurements were taken both outside the transects and beyond the boundaries of Hester Marsh during two post-fire survey periods: post-fire#1 (21 January–12 February 2025) and post-fire#2 (18 February–27 March 2025) (see Supplementary Sect. 1). These post-fire surveys encompassed a broader area, including nearby grasslands within the surrounding watershed (Fig. 2). This approach incidentally enabled differentiation of recent fire-related metal deposition from background levels and allowed detection of a transient, spatially patchy signal. All FpXRF measurements across all surveys have been conducted on bare, relatively dry soils to minimize moisture-related biases.

			Surface												Subsurface†											
			Ni (ppm)				Mn (ppm)				Co (ppm)				Ni (ppm)				Mn (ppm)				Co (ppm)			
Survey period	Sites (*n*)	Area (km²)	min	max	median	MAD	min	max	median	MAD	min	max	median	MAD	min	max	median	MAD	min	max	median	MAD	min	max	median	MAD
Pre-fire (2023)	97	0.4	52	246	109	47	228	2193	713	315	72	298	183	59	52	232	116	43	324	2378	834	303	59	214	107	43
Post-fire#1 2025*	135	5.6	52	3702	441	517	386	7119	1488	783	40	1604	309	296	50	303	93	44	264	2119	926	435	40	218	91	49
Post-fire#2 2025^	64	5.6	52	339	100	49	45	3207	871	551	8	833	107	68	1	329	100	49	45	3207	871	551	8	265	97	56

Table . Summary statistics including minimum and maximum values, median, and median absolute deviation (MAD) of nickel (Ni), manganese (Mn), and Cobalt (Co) concentrations (ppm) in surface and subsurface soils measured by field-portable XRF (FpXRF) across three survey periods. Values represent minimum, maximum, and mean concentrations for each metal. †Subsurface measurements are from a few mm below the surface; *Post-fire#1 survey conducted Jan 21–Feb 12; ^Post-fire#2: Feb 18–Mar 27 (surface samples were measured in triplicate during Post-fire#2).

Soil samples collected in the field were analyzed using the pXRF in the lab (LpXRF) and with inductively coupled plasma mass spectrometry (ICP-MS) (Table S3).

Detailed laboratory procedures, including sample preparation, organic carbon analysis, and instrument protocols, environmental data, as well as statistical methods used for data analysis (non-parametric pairwise tests and regression analysis) and interpretation are provided in Supplementary Sect. 2.

Rain and tide data were retrieved from the Moss Landing weather station operated by Moss Landing Marine Laboratories and wind data from the ESNERR meteorological station (Tables S4 and S5).

Results

Detection and mapping of the cathode metals

Fragments of ash and burned or charred material were found scattered across Hester Marsh soils (Fig. 1b, c) in the days to weeks after the fire, providing clear physical evidence of fallout from the battery fire. The comparison between the 2023 and the 2025 post-fire data revealed a marked increase in concentrations of three metals: nickel (Ni), manganese (Mn), and cobalt (Co).

Notably, surface Ni and Co co-varied on log–log axes, with post-fire Ni: Co ratios averaging 2:1, consistent with NMC532 cathode chemistry. This fingerprint supports attribution of the (Ni, Mn, Co) metal spike to battery fire fallout.

Further analysis of selected samples using scanning electron microscopy (SEM) and energy-dispersive X-ray spectrometry (EDS) indicated that the elevated concentrations of Ni, Mn, and Co were linked to the presence of micron-sized metallic particles like those used as cathode materials in Nickel Manganese Cobalt (NMC) batteries. At finer scales, cathode-derived NMC microparticles were identified and elementally mapped in surface soil samples using SEM/EDS (Fig. 1d, e, f), consistent with the fracture and ejection of individual grains from NMC cathodes, a behavior previously observed in laboratory combustion tests[6]. These findings confirm the presence of fire-related battery material on the soil surface of nearby wetlands.

Geochemical evidence from FpXRF further supports the extent and magnitude of contamination. Although Ni, Mn, and Co displayed high spatial variability during the post-fire#1 survey, concentrations increased significantly relative to pre-fire values, with maximum Ni rising by an order of magnitude and Co by a factor of five (Table 1).

Overall, by the time the post-fire#2 survey was conducted, about 1 month after the battery fire, the median concentrations had decreased. The post-fire#1 subsurface data were statistically indistinguishable from the surface and subsurface 2023 pre-fire data. In contrast, surface concentrations of (Ni, Mn, Co) measured during the post-fire#1 survey were significantly elevated compared to pre-fire levels ($p < 0.001$, Mann–Whitney U test; Table S6), clearly indicating that the deposition associated with the fire was initially confined to the top layer of soil.

Figure 2 show that the post-fire#1 increase in metal concentrations (Ni, Mn, Co) in surface measurements was not uniform but clustered in distinct hotspots within Hester Marsh. Hester Marsh was also the area where the post-fire#2 survey recorded the most substantial decrease in metal concentrations. However, a few locations continued to show elevated levels, which explains why the maximum values of Ni and Co in the post-fire#2 survey remained high (Table 1). In contrast to the surface measurements, subsurface data showed no significant changes in either mean or maximum concentrations between the pre- and post-fire surveys. This further confirms that the sharp post-fire increase in cathode metal concentrations was confined to the topmost layer of the soil.

Although the FpXRF measurement along three permanent transects included the concentrations of all three cathode elements: Ni, Mn, and Co, we focused primarily on Ni as a tracer of battery fire fallout, as Ni is dominated by a single oxidation state (Ni^{2+}) across a broad range of redox and pH conditions. This makes it less sensitive to post-depositional remobilization compared to Mn and Co, both of which exhibit variable redox behavior in estuarine settings[13].

Mn is strongly influenced by fluctuations in redox potential and organic matter, and its concentrations often vary independently of anthropogenic inputs[14]. Co also exhibited substantial redox sensitivity and, notably, a large proportion of Co measurements were non-detects, especially in pre-fire and subsurface samples (Table S7), due to concentrations below the portable XRF instrument's relatively high detection limit (Ni ≈ 50 ppm, Mn ≈ 45 ppm, Co ≈ 40 ppm). Box plots depicting the temporal trends of surface Ni concentrations at three permanent transects show that, following the fire, the median Ni concentration increased by two to threefold compared to pre-fire levels (Fig. 3). Over the month-long survey period, both the median and interquartile range of concentrations declined, with a substantial drop to near pre-fire values observed in early February coincident with rainfall in the area. Notably, Ni concentrations rose again at all transects during the surveys conducted in the second half of February.

On log–log axes (Fig. 4a), surface Ni and Co show clear bivariate associations. The distribution of $\log_{10}$(Ni/Co) (Fig. 4b) shows that post-fire values average near the 2:1 reference (0.301), while pre-fire values average < 0 indicating a substantial change in surface soil metal composition following the fire.

Comparative elemental analysis: field versus lab

To compare FpXRF results with laboratory measurements, we collected 51 samples (24 subsurface and 27 surface) from soils that had previously been analyzed in the field with FpXRF after the battery fire. Aliquots of these samples were analyzed for moisture content, organic carbon content, and elemental composition using LpXRF (5–6 g) and ICP-MS (~ 0.25 g). The water content of the samples ranged from approximately 7 to 43% by weight, while organic carbon concentrations varied between 0.1% and 2.4% by weight.

Because regressions of XRF against the ICPMS reference had non-zero intercepts and modest R^2, we quantified method bias as the geometric mean of the per-sample ratios (i.e., FpXRF/ICPMS, LpXRF/ICPMS, and for completeness FpXRF/LpXRF, see Table S8). In subsurface samples, both XRF methods overestimated Ni

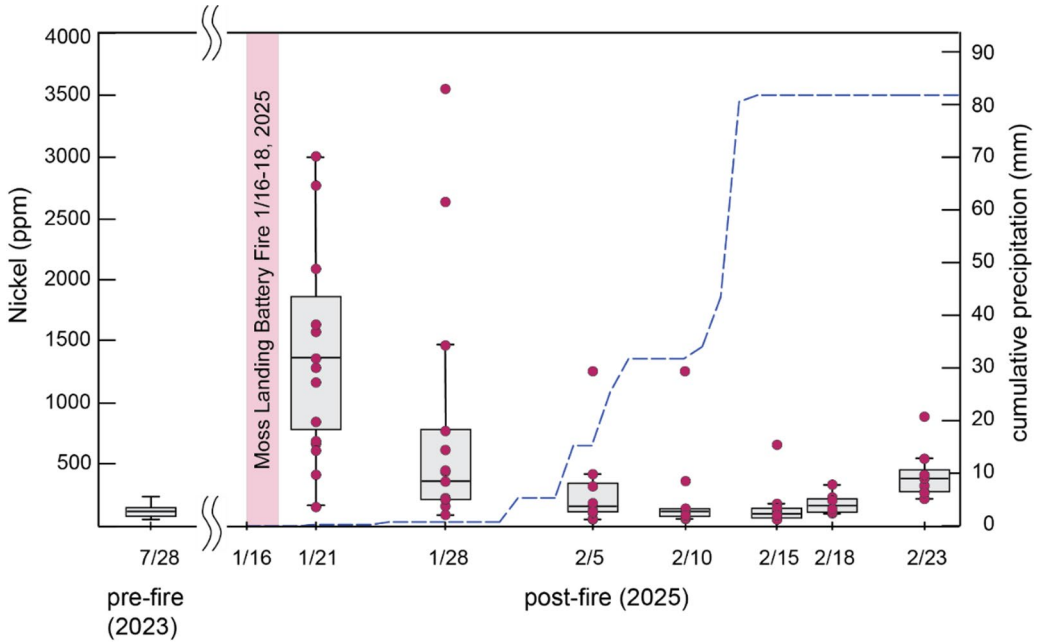

Fig. 3. Temporal variability in surface nickel (Ni) concentrations (ppm) along three permanent transects measured before the battery fire in 2023, and between January and February 2025 using field-portable X-ray fluorescence (FpXRF). Box plots represent the distribution of Ni concentrations at the benchmarks along each transect measured during each sampling date. The datapoints are represented with red circles (the pre-fire survey data were not included because they were indistinguishable and overlapping given their low values). The dashed line shows cumulative precipitation data recorded at the Moss Landing Marine Laboratories weather station (Latitude: 36.80040° N, Longitude: 121.78842° W). A transient spike in Ni concentrations occurred immediately after the 16 January 2025 battery fire, followed by a rapid decline, likely associated with rainfall and tidal flushing in early February. A smaller secondary increase was observed in late February, coinciding with the 18 February 2025 reignition event.

relative to ICPMS by roughly threefold (FpXRF/ICPMS = 3.09, 95% CI 2.74–3.48; LpXRF/ICPMS = 2.81, 95% CI 2.61–3.02), while the two types of XRF measurements were in reasonable agreement (FpXRF/LpXRF = 1.10, 95% CI 0.97–1.25). In surface samples, both FpXRF and LpXRF exhibited a larger positive bias (FpXRF/ICP-MS = 5.40, 95% CI 4.18–6.99; LpXRF/ICP-MS = 2.33, 95% CI 1.93–2.81). As we describe below, the stronger disagreement between FpXRF and laboratory measurements at the surface is best explained by dilution of a thin, metal-rich veneer during laboratory homogenization (which mixes surface material with underlying soil), whereas in-situ FpXRF interrogates the veneer more directly.

As observed with FpXRF data, LpXRF measurements of subsurface samples showed no significant linear association between Co and Ni. In contrast, surface samples showed coherent Ni–Co covariation across methods; Ni: Co ratios were near 2:1, consistent with Fig. 4b and the Ni-to-Co ratio observed in the post-fire#1 FpXRF survey data (Table S9).

Depth distribution of cathode metals

The NMC microparticles primarily occurred as aggregates of varying shape and size, often ~ 100 µm or larger (Fig. 1d, f). This suggests a minimum thickness for the deposition layer of approximately 100 µm, comparable to the critical detection depths for Ni, Mn, and Co in XRF analysis, defined as the depth beyond which less than 1% of the original fluorescent signal reaches the detector.

A rough estimate of the thickness of this contaminated layer can be derived by comparing FpXRF measurements with LpXRF results from sliced surface samples for which lab-based measurements using both LpXRF and ICP-MS yielded lower concentrations of Ni, Mn, and Co compared to those obtained via FpXRF.

Our hypothesis was that FpXRF and LpXRF should approximately yield similar concentrations (i.e., FpXRF/LpXRF ≈ 1) only when the thickness of the lab-analyzed sample approaches the depth of the metal-enriched layer. If the sample is thicker, it will include subsoil not affected by the fire, diluting the signal and resulting in FpXRF/LpXRF > 1.

A regression analysis of sample thickness versus the FpXRF/LpXRF ratio revealed a moderate positive linear association ($R^2 = 0.30$, $p = 0.0129$) that should be interpreted with caution. However, the ratio approaches one for samples between ~ 2 and 5 mm thick, which we interpret as the approximate depth to which fire-related cathode metals were initially incorporated into the soil (Figure S3).

This finding is consistent with our surface method comparison against the ICPMS reference: as the effective field sampling depth increases, the measured signal is increasingly diluted by pre-fire baseline material, leading

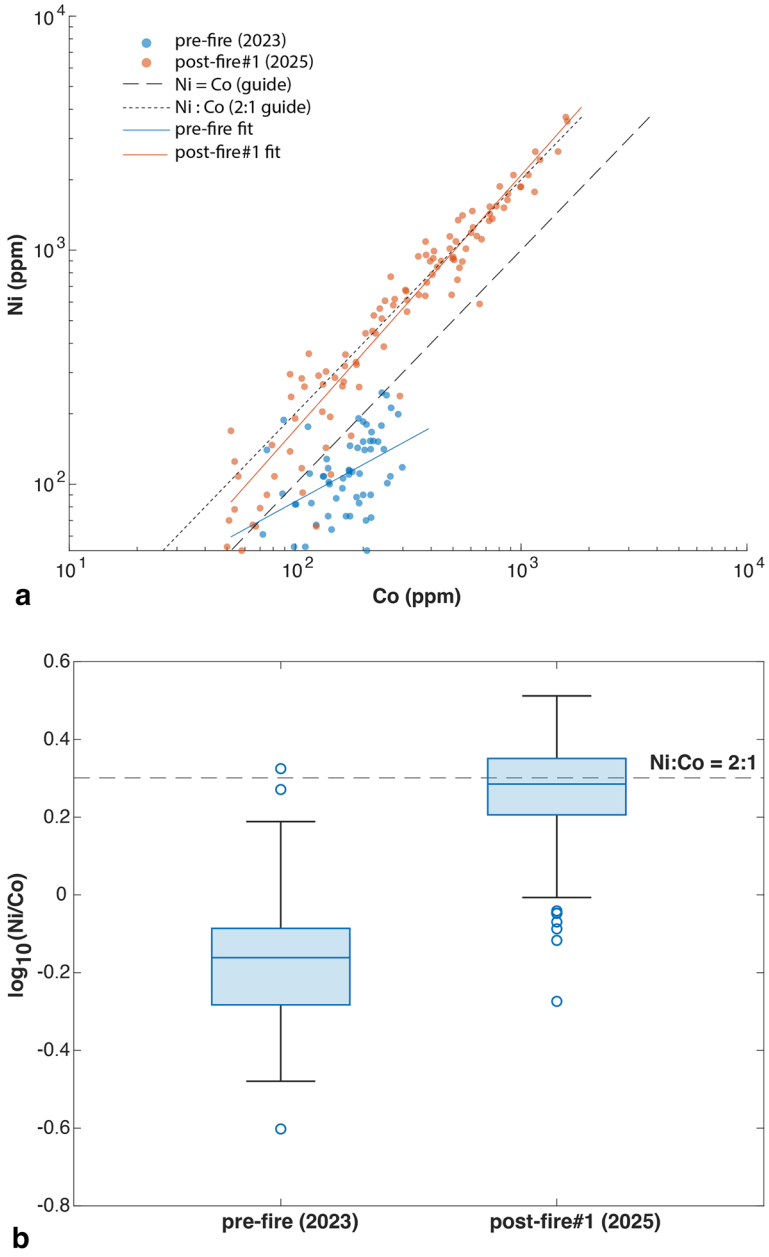

Fig. 4. (**a**) Log–log scatter of Co versus Ni (ppm; FpXRF) for pre-fire (2023, blue) and post-fire#1 (Jan–Feb 2025, orange). Guidelines show Ni = Co (1:1) and Ni: Co = 2:1. Robust log–log fits: pre b = 0.45 (95% CI 0.25–0.65); post b = 0.85 (0.80–0.89). (**b**) Distributions of $\log_{10}$(Ni/Co) for the same samples; dashed line at 0.301 marks Ni: Co = 2:1. Post-fire medians lie near 2:1, whereas pre-fire values are < 0.

to underestimation of battery fire-related surface contamination (see Supplementary Sect. 2 for a detailed discussion of pXRF detection depth and matrix effects).

Discussion

Rapid detection of cathode metals with FpXRF

The sharp increase in (Ni, Mn, Co) metal concentrations detected in the surface soils of Hester Marsh between late January and early February 2025 is clearly attributable to the deposition of particulate matter from the smoke plume generated by the nearby battery storage facility fire at Moss Landing just days earlier. This interpretation is supported by multiple lines of evidence, including visible ash residues and soot, the presence of cathode-derived microparticles in surface soils, and distinctive geochemical patterns.

The key to early detection of cathode metal fallout immediately after the Moss Landing battery fire was the use of FpXRF. While field measurements were not as accurate as lab measurements, they played a pivotal role in rapidly observing that maximum concentrations of the three metals increased by an order of magnitude after the fire, monitoring how quickly they decreased, and assessing how patchy the battery metal fallout was across

the landscape. This key information could have been completely missed if we had relied only on a handful of samples taken in space and time. Metal co-variation patterns were consistent across methods (FpXRF, LpXRF, ICP-MS), while absolute levels differed.

While the use of FpXRF offers substantial advantages in responding quickly to environmental emergencies like battery fires, it also comes with limitations. These are especially pronounced in wetland soils, where moisture content, organic matter, and textural variability can significantly influence the accuracy of XRF readings. Light elements such as Ni, Mn, and Co are particularly susceptible to overestimation when measured with XRF, compared to more precise ICP-based methods[15–18]. Our comparison of field and laboratory measurements confirms this pattern: both FpXRF and LpXRF overestimated Ni concentrations by more threefold relative to ICP-MS in the subsurface where samples do not include the fallout deposit.

Nevertheless, the methods showed an acceptable level of reproducibility, supporting the reliability of XRF for rapid environmental assessment. Importantly, although absolute concentrations may be overestimated, the change in surface concentrations before and after the fire was evaluated using the same FpXRF method, allowing for robust spatial comparison and comparison of relative differences over time.

A fingerprint for the cathode material

On log–log axes, Ni scales with Co in surface soils (Fig. 4a). Using ordinary least squares (OLS), the pre-fire fit yields b = 0.4750b and a = 0.9913 ($R^2 = 0.175$), indicating a heterogeneous pre-fire ambient signal. The post-fire (survey 1) yields b = 1.1023 and a = 0.0061 ($R^2 = 0.912$); the point cloud and fitted line lie close to the Ni = 2·Co guideline across the observed range, motivating a ratio view.

Figure 4b shows that the distribution of $\log_{10}$(Ni/Co) shifts from pre-fire values < 0 (Ni: Co < 1) to post-fire values near the 2:1 reference ($\log_{10}2 = 0.301$). This composition is consistent with the NMC532 cathode chemistry used in lithium-ion batteries[19].

Subsurface samples remained near pre-fire levels and did not exhibit the post-fire ratio shift, indicating enrichment confined to a surface veneer. Notably, maximum surface concentrations of all three metals increased by several fold relative to pre-fire levels (Table 1). Most post-fire#1 surface samples analyzed with ICP-MS had Ni concentrations above 50 ppm, values that exceed thresholds associated with toxicity risks to plants and aquatic organisms[20].

The observed changes in surface concentrations of Ni, Mn, and Co across Hester Marsh and surrounding areas over time indicate the potential for rapid remobilization of these transition metals into estuarine soils and downstream waters (Fig. 2). FpXRF transect data from February–March 2025 show that surface Ni concentrations dropped to near baseline within weeks of the fire, following early February rain and tidal inundation (Fig. 3).

While variability in Ni concentrations declined over time, indicating redistribution of the cathode metals, at the higher elevation transect T12 (~ 1 km from the fire), higher Ni levels persisted for about 10 days before declining, while the lower elevation transects T3 and T8 showed an earlier decrease, likely due to January tidal flooding that immersed only the areas with the lowest relief.

The transect data and a simple comparison between columns 2 and 3 in Fig. 2 illustrate that had FpXRF sampling been delayed by even a few days, most of the early evidence for surface deposition in Elkhorn Slough would likely have been lost. Timely field deployment was essential for capturing the initial contamination signal before environmental processes such as rainfall and tidal flushing remobilized the metals.

Our results emphasize the high degree of spatial variability in the distribution of battery-associated metals on the soil surface. The highest concentrations observed after the fire were within the unvegetated portions at Hester Marsh (Fig. 2). Concentrations were also highly variable at finer spatial scales, between samples collected 10–20 m apart along the transects.

Boxplots of Ni concentrations over time along three transects (Fig. 3) show that the interquartile range, a measure of variability excluding outliers, increases with the median concentration. This relationship suggests that spatial heterogeneity is greatest where concentrations are highest, a pattern we interpret as evidence of the clumped distribution of cathode metal-bearing particles or ash. At the microscale, this clumping is represented by aggregates of NMC microparticles (Fig. 1d–f); at the macroscale, it is reflected in the scattering of ash and burned material fragments observed throughout the study area, up to approximately 3 km from the battery storage facility (Fig. 1b, c). Larger clumps result in higher localized concentrations and contribute to measurement variability, reinforcing the importance of repeated sampling at multiple spatial scales. This multi-scale capability is one of the key advantages of FpXRF over conventional discrete sampling and ensuing analysis via ICP-MS.

The relationship between the FpXRF/LpXRF concentration ratio and sample thickness used to estimate the critical depth of Ni enrichment following the battery fire shows that the ratio approaches 1.0 when sample thicknesses range between ~ 2 and 5 mm, suggesting that most of the deposited Ni was confined to the uppermost few millimeters of soil. Thicker samples diluted this surface signal, consistent with a sharp depositional pulse and limited vertical mixing. This interpretation aligns with both SEM imaging of NMC microparticle aggregates and the shallow critical escape depth of Ni in soil matrices.

Tracking the environmental footprint of cathode material

The cathode material detected in Elkhorn Slough soils following the battery fire was, at least initially, airborne. As a first approximation, the spatial distribution of cathode metals observed in surface soils during the post-fire#1 survey reflects the deposition pattern of battery-derived particulates that settled from the smoke plume. However, this interpretation likely oversimplifies the dynamics. Prior studies show that ground-level deposition often diverges from the plume's direction due to complex atmospheric behavior, as additional factors might be influencing spatial variability including plume height, particle size and shape, and sorptive properties of the soil surface[21,22].

Our reconstruction of the (Ni, Mn, Co) metal distribution from the post-fire#1 survey reveals that surface concentrations of contaminants do not increase with proximity to the battery fire site. Instead, concentrations peak in the Hester Marsh wetland, located approximately 1–3 km east of the facility (Fig. 2). This offset may be explained by westerly surface winds on the day of the fire, which prevailed for approximately 40% of the time, likely directing the smoke plume eastward over Hester Marsh (Fig. 1a). In addition to wind direction, local soil characteristics may have played a role in the retention of the metal particles following deposition. Hester Marsh soils are predominantly fine-grained and clay-rich, with high sorptive capacity, and higher potential for retention of transition metals that can increase their persistence in surface layers[23,24].

Regardless of the factors that controlled the initial distribution and retention of material deposited from the battery fire, the spike in transition metal concentrations at the surface of the wetland was short-lived. By the time the post-fire#2 survey was conducted, most of the cathode metals accumulated on the surface soils had been remobilized, except for a few persistent hotspots in some of the depressional salt pans within Hester Marsh (Fig. 2).

Natural processes such as rainfall and tidal inundation likely played a major role in the resuspension and remobilization of the contaminants. Precipitation was relatively intense during the first 2 weeks of February 2025 (Fig. 3), and the lower portions of Hester Marsh experienced repeated inundation during high-tide events, facilitating the physical transport and dispersal of deposited cathode metals. Percolation through the soils appears to have been limited since the post-fire#2 and post-fire#1 subsurface concentrations were statistically indistinguishable.

The drop in surface concentration of cathode metals resulting from the battery fire strongly suggests that the metals have been washed into downstream portions of the estuarine ecosystem. Their transport and fate throughout the estuary and potentially into adjacent open coastal ecosystems remain unknown. They may have settled in tidal channels, become buried in sediments, or undergone chemical transformations driven by redox cycling[25].

These processes could affect both metal mobility and, over time, pose a threat to higher trophic levels through bioaccumulation. Ni, Mn, and Co are all known to be toxic to humans as well as to aquatic and terrestrial organisms[20], and Mn toxicity is a major constraint limiting plant growth and production[16]. Co can have lethal or sublethal effects on reproduction in fish and crustaceans and has some bioaccumulation potential through adsorption to plant roots[26]. These risks are particularly acute at Hester Marsh, where an $18 M investment to restore tidal wetlands through soil augmentation raised marsh platforms to elevations intended to sustain native plant growth and survival under future flooding[27].

Mass budget for cathode metal deposition at Hester Marsh

The initial mass of Ni, Mn, and Co originating from the burned batteries that settled on Hester Marsh can be estimated based on the difference between metal concentrations measured at the surface during the pre-fire and the post-fire#1 surveys (see Table S10 for full calculations). To calculate the mass budget, the Hester Marsh area (1200,000 m^2) was overlain with a 200 × 200 m grid composed of 30 cells, each covering a 40,000 m^2 area. For 10 of the 30 cells that contained both pre-fire and post-fire#1 FpXRF measurements, we computed the paired mean difference (post-fire#1—pre-fire) and the standard errors. The concentrations of the three metals were then converted to mass assuming a surface contamination depth of approximately 0.1 mm (which approximates the critical detection depth for these metals) and a dry density of 1500 kg/m^3 for consolidated clay.

We estimate that the minimum deposited mass of cathode metals within the upper 100 μm is ~ 17 kg ± 4 kg per 200 × 200 m cell. However, as discussed earlier, the actual thickness of the soil layer containing the deposited metals is likely greater than the effective depth, and can be ~ 5 mm thick, which corresponds to a mass of cathode metals of ~ 855 kg ± 199 kg per cell. Extrapolation to the entire Hester Marsh area yields an estimated total mass of cathode metals of ~ 25 metric tons (25676 kg ± 5981 kg).

This estimate should be interpreted with caution. First, FpXRF measurements overestimate Ni concentrations by a factor of ~ 3, and the metal concentrations are expected to decline with depth due to dilution and limited vertical mixing. However, the values are also conservative, as they only include deposition on bare soil and exclude potential accumulation on vegetation, which may represent a larger surface area in marsh and upland settings than the exposed soil itself.

To put these figures in perspective, a 1 MW industrial lithium-ion battery manufactured by LG weighs 1.6 metric tons, with cathode materials accounting for approximately 35% of the total mass. This equates to roughly 1900 metric tons for the entire 1200 MWh storage capacity of the Moss Landing facility. If, as reported by Monterey County officials[10], approximately 75% of the batteries were destroyed in the fire, then an estimated ~ 1400 metric tons of cathode material could have been involved in the event and potentially entrained into the smoke plume. Therefore, our estimates of the total mass of (Ni, Mn, Co) metals deposited on the soils of the Hester Marsh extrapolated to a 5 mm cathode metal deposit accounts only for < ~ 2% of the total battery material that may have been released during the Moss Landing battery fire.

Conclusions and implications for future battery fire response

To our knowledge, this study represents the first field-based documentation of battery-associated metal fallout following a large-scale lithium-ion battery fire and offers a framework for assessing future events of this kind. Use of field instrumentation enabled immediate collection of hundreds of measurements, critical given the spatial patchiness of battery metal aggregates in an extensive fallout layer in the vicinity of the fire and given the rapidity with which the metals were transported downstream by tides and rain. As battery energy storage systems continue to expand in scale and density, the risk of both localized and widespread contamination will increase even as safety protocols improve.

This incident also calls attention to the limitations of standard environmental sampling protocols. Conventional soil sampling depths, such as the commonly used top ~ 6 cm of soil[28], may fail to detect thin, spatially heterogeneous deposition layers. The patchy nature of ash deposition observed in this study suggests that sampling strategies must be adaptive and designed to capture contamination at multiple spatial scales and depths. This is especially critical in the first few days following an event, since, over time, rainfall, tides, and wind can rapidly redistribute surface-bound contaminants.

Environmental response frameworks must also consider the potential offset between fire origin and deposition zones. In this case, the most significant contamination occurred not adjacent to the site of the fire, but several kilometers downwind. This spatial offset highlights the need for evacuation protocols and monitoring networks that integrate plume dispersion models, meteorological data, air quality monitoring and ground-based measurements of deposition.

Finally, findings from controlled laboratory battery burns provide additional context for interpreting field observations. Previous experiments have demonstrated that thermal decomposition of cathode materials can release substantial quantities of (Ni, Mn, Co) metals and other toxicants[6]. These studies confirm that NMC-based batteries, when subjected to fire conditions, can emit airborne particles capable of traveling significant distances before settling onto the landscape. Field studies such as this one are essential to understanding how such deposition events unfold under real-world conditions.

Together, these results emphasize the need for proactive planning, site-specific risk assessment, and rapid, multi-scale environmental monitoring in the aftermath of battery fires. As battery technologies evolve, so too must the frameworks we use to track and mitigate their potential environmental impacts.

Data availability

All data used to generate the figures are available through Figshare at https://figshare.com/s/32fb2899e519353f923b **.**.

Received: 14 August 2025; Accepted: 27 October 2025
Published online: 26 November 2025

References

1. Koohi-Fayegh, S. & Rosen, M. A. A review of energy storage types, applications and recent developments. *J. Energy Storage* **27**, 101047. https://doi.org/10.1016/j.est.2019.101047 (2020).
2. Gutsch, M. & Leker, J. Global warming potential of lithium-ion battery energy storage systems: A review. *J. Energy Storage* **52**, 105030. https://doi.org/10.1016/j.est.2022.105030 (2022).
3. Gür, T. M. Giga-ton and tera-watt scale challenges at the energy-climate crossroads: A global perspective. *Energy* **290**, 129971. https://doi.org/10.1016/j.energy.2023.129971 (2024).
4. Armand, M. et al. Lithium-ion batteries—current state of the Art and anticipated developments. *J. Power Sources* **479**, 228708. https://doi.org/10.1016/j.jpowsour.2020.228708 (2020).
5. Xie, J., Li, J., Wang, J., Jiang, J. & Shu, C. M. Fire risk assessment in lithium-ion battery warehouse based on the bayesian network. *Process. Saf. Environ. Prot.* **176**, 101–114. https://doi.org/10.1016/j.psep.2023.06.005 (2023).
6. Barone, T. L. et al. Lithium-ion battery explosion aerosols: Morphology and elemental composition. *Aerosol Sci. Technol.* **55**, 1183–1201. https://doi.org/10.1080/02786826.2021.1938966 (2021).
7. Mrozik, W., Rajaeifar, M. A., Heidrich, O. & Christensen, P. Environmental impacts, pollution sources and pathways of spent lithium-ion batteries. *Energy Environ. Sci.* **14**, 6099–6121. https://doi.org/10.1039/D1EE00691F (2021).
8. Lopez, R. D. *Ramsar Wetlands of the North American West Coast and Central Pacific: An Atlas* (CRC, 2024). https://doi.org/10.1201/9781003046394
9. Vistra Corp. Vistra completes expansion of battery energy storage system at its flagship California facility. https://investor.vistracorp.com/2021-08-19-Vistra-Completes-Expansion-of-Battery-Energy-Storage-System-at-its-Flagship-California-Facility (Accessed 29 September 2025).
10. San Francisco Chronicle. Fire at California battery plant brings safety assurances, quest for answers. San Francisco Chronicle (18. Jan (2025). https://www.sfchronicle.com/california/article/moss-landing-fire-20042587.php (Accessed 29 September 2025).
11. County of Monterey. Moss Landing Power Plant Fire. https://www.readymontereycounty.org/emergency/2025-moss-landing-vistra-power-plant-fire (Accessed 29 September 2025).
12. Van Dyke, E. & Wasson, K. Historical ecology of a central California estuary: 150 years of habitat change. *Estuaries* **28**, 173–189. https://doi.org/10.1007/BF02732853 (2005).
13. Yang, Z., Guo, W., Fan, Y., Lin, C. & He, M. High-resolution profiles of iron, manganese, cobalt, cadmium, copper and zinc in the pore water of estuarine sediment. *Int. J. Environ. Sci. Technol.* **10**, 275–282. https://doi.org/10.1007/s13762-012-0110-2 (2013).
14. Bartlett, R. J. Manganese redox reactions and organic interactions in soils. In Manganese in Soils and Plants (eds (eds Graham, R. D., Hannam, R. J. & Uren, N. C.) 59–73 (Springer, Dordrecht, 1988). https://doi.org/10.1007/978-94-009-2817-6_5
15. Sikora, A. L., Maguire, L. W., Nairn, R. W. & Knox, R. C. A comparison of XRFS and ICP-OES methods for soil trace metal analyses in a mining-impacted agricultural watershed. *Environ. Monit. Assess.* **193**, 92. https://doi.org/10.1007/s10661-021-09275-9 (2021).
16. Li, W. et al. Comparative study on the determination of heavy metals in soil by XRF and ICP-MS. *J. Phys. : Conf. Ser.* **2009** (012075). https://doi.org/10.1088/1742-6596/2009/1/012075 (2021).
17. Ge, L., Lai, W. & Lin, Y. Influence of and correction for moisture in rocks, soils and sediments on in situ XRF analysis. *X-Ray Spectrom.* **34**, 28–34. https://doi.org/10.1002/xrs.782 (2005).
18. Wilson, P., Cooke, M., Cawley, J., Giles, L. & West, M. Comparison of the determination of copper, nickel and zinc in contaminated soils by X-ray fluorescence spectrometry and inductively coupled plasma spectrometry. *X-Ray Spectrom.* **24**, 103–108. https://doi.org/10.1002/xrs.1300240305 (1995).
19. ECHA. Lithium nickel cobalt manganese oxide. European Chemicals Agency. https://echa.europa.eu/ (Accessed 29 September 2025).
20. Eisler, R. Nickel hazards to fish, wildlife, and invertebrates: A synoptic review. US Geological Survey, Patuxent Wildlife Research Center. https://restservice.epri.com/publicdownload/000000003002030360/0/Product (Accessed 29 September 2025).
21. Lejon, C. et al. Lagrangian plume rise and dispersion modelling of the large-scale lithium-ion battery fire in Morris, USA, Air Qual. Atmos. Health 17, 2077–2089 (2024). https://doi.org/10.1007/s11869-023-01443-9 (2021).
22. Goodrick, S. L., Achtemeier, G. L., Larkin, N. K., Liu, Y. Q. & Strand, T. M. Modelling smoke transport from wildland fires: A review. *Int. J. Wildland Fire* **22**, 83–94. https://doi.org/10.1071/WF11116 (2013).

23. Shand, C. A. & Wendler, R. Portable X-ray fluorescence analysis of mineral and organic soils and the influence of organic matter. *J. Geochem. Explor.* **143**, 31–42. https://doi.org/10.1016/j.gexplo.2014.03.005 (2014).
24. Kravchenko, E. et al. Ecological and health risk assessments of heavy metal contamination in soils surrounding a coal power plant. *J. Hazard. Mater.* **484**, 136751. https://doi.org/10.1016/j.jhazmat.2024.136751 (2025).
25. Barrio-Parra, F. et al. Environmental risk assessment of Cobalt and manganese from industrial sources in an estuarine system. *Environ. Geochem. Health* **40**, 737–748. https://doi.org/10.1007/s10653-017-0020-9 (2018).
26. ATSDR. Toxicological Profile for Cobalt. https://www.atsdr.cdc.gov/toxprofiles/tp33.pdf (Accessed 29 September 2025).
27. Haskins, J. et al. UAV to inform restoration: A case study from a California tidal marsh. *Front. Environ. Sci.* **9**, 642906. https://doi.org/10.3389/fenvs.2021.642906 (2021).
28. US EPA. Method 6200: Field portable X-ray fluorescence spectrometry for the determination of elemental concentrations in soil and sediment. https://www.epa.gov/sites/default/files/2015-06/documents/6200.pdf (Accessed 29 September 2025).

Acknowledgements

We are deeply grateful to Julie Packard, Nancy Burnett, and Louise Stephens for their generous support and long-standing commitment to environmental research and conservation. We also thank the Monterey Bay Aquarium and the Simpkin Family for their crucial contributions, which made this work possible. Their support has been instrumental in enabling rapid response science and advancing our understanding of environmental risks in estuarine ecosystems. A grant from NOAA's Office for Coastal Management in support of the Elkhorn Slough National Estuarine Research Reserve (ESNERR) provided funding for KW and CE. The fortuitous pre-fire baseline was made possible due to ESNERR's heavy investment in restoration monitoring at Hester Marsh with grants from the California Department of Fish and Wildlife Greenhouse Gas Reduction Program, Ocean Protection Council and USFW National Coastal Wetland Program. The majority of data for this study come from ESNERR, a partnership between California Department of Fish and Wildlife and NOAA, and we are grateful for ESNERR's support of the study. We acknowledge MLML/Marine Pollutions Study Lab staff members Autumn Bonnema, Adam Newman, and April Sjoboen Guimaraes for ICP-MS sample digestions and analysis. Two anonymous reviewers provided thoughtful suggestions that improved the presentation of data and the clarity of writing.

Author contributions

I.W.A conceived the study, led the writing and contributed to all aspects of this work; CE performed field work, data collection and geospatial interpretations; SC performed lab analyses; MF contributed to study design, site access and data collection; MG contributed to data interpretation; WH performed lab analysis and data interpretation; AK contributed to data interpretation; KW contributed to study design, site access and data interpretation. All authors contributed to manuscript revisions and approved the final version.

Declarations

Competing interests

The authors declare no competing interests.

Additional information

Supplementary Information The online version contains supplementary material available at https://doi.org/10.1038/s41598-025-25972-8.

Correspondence and requests for materials should be addressed to I.W.A.